Mini-FDPM: a Handheld Non-Invasive Breast Cancer Detector Based on Frequency Domain Photon Migration

Keun Sik No, Pai H. Chou
Department of EECS, University of California, Irvine, CA 92697-2625 USA
{*kno,phchou*}*@uci.edu*

Abstract

Mini-FDPM is a handheld system for noninvasive breast cancer detection based on frequency domain photon migration. It performs broadband modulation on near-infrared laser intensity and derives the scattering and absorption coefficients from phase and amplitude measurements. It overcomes many challenges in broadband and optical driver circuitry. Measurements show Mini-FDPM outperforms the current prototype while costing a small fraction.

1 Introduction

FDPM, for frequency domain photon migration spectroscopy [1], is a new way of detecting breast cancer. This paper reports on a handheld unit, called Mini-FDPM, constructed using entirely conventional discrete components. It achieves higher performance, lower power, and smaller form factor at only a small fraction of the cost.

1.1 Common and Experimental Techniques

Mammography is most common, but besides discomfort, X-ray can pose new health risks. Magnetic resonance imaging (MRI) requires long session time, is costly and not applicable to patients with pacemakers or surgical metal clips. Ultrasound cannot detect early cancerous signs that show on mammograms. Positron emission tomography (PET) and impedance scanning are often invasive, requiring insertion of a probe into the patient. Microwave tomography [2] measures reflection of ultra-wideband microwave pulses [3, 4], but require a special tank to immerse the breast and cannot distinguish between benign and malignant tumors [5].

1.2 FDPM

FDPM overcomes the limitations of existing techniques by beaming near-infrared (NIR) light (600nm $\leq \lambda \leq$ 1300nm) and measuring its reflection. The NIR light is modulated with RF frequency from 10 MHz to 1 GHz. The phase shift and amplitude responses of the breast tissue define a "signature" that can help detect tumors [1]. FDPM is fast, robust, non-invasive. The laser light used is less energetic than visible light, and thus FDPM presents a low-risk, low-cost alternative to ionizing radiations. Because it is content-based rather than image-based, it can reduce misdiagnosis due to errors in manual inspection or image processing.

1.3 FDPM Instrument

FDPM has been in clinical trial at the Beckman Laser Institute (BLI) for several years with large volumes of data. Researchers at BLI built the laser breast scanner (LBS) using an HP 8753C network analyzer [6] for both signal generation and data acquisition. A computer post-processes the data by running a series of equations and plots graphs of absorption and scattering in the tissue. However, this setup is expensive, costing over $100,000. By specialization and leveraging off-the-shelf technologies for broadband communications and computers, Mini-FDPM is not only higher performance but also much lower cost.

2 Mini-FDPM System

Fig. 1(a) shows Mini-FDPM consisting of a wideband signal generator, laser modulator, and detector. The signal generator modulates the amplitude of laser light with RF frequency from 10MHz to 1GHz in 10MHz steps and can adjust steps from 500kHz. The signal is amplified and drives the laser diode after a DC-bias. The photo detector converts the reflected light into an RF signal, and the amplitude and phase detector compares it against the reference signal. An 8-bit microcontroller samples the amplitude and phase data and generates the next frequency. The power of output are controllable via programmable attenuators.

2.1 Signal Generator

To produce 10MHz–1GHz signals, we mix a fixed, 2.5GHz frequency with a 1.5–2.49GHz band. To get a precise frequency, a PLL (Phase Locked Loop) is needed. We use a frequency synthesizer, which divides the VCO (voltage controlled oscillator) signal and compares the frequency against a temperature compensated crystal oscilla-

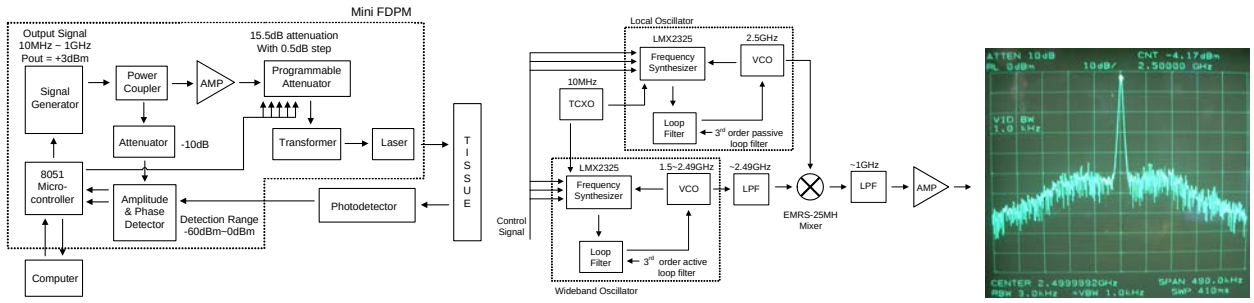

(a) (b) (c)

Figure 1: (a) Topology of Mini-FDPM Device (b) Topology of Signal Generator (c) Phase Locked Frequency at 2.5GHz.

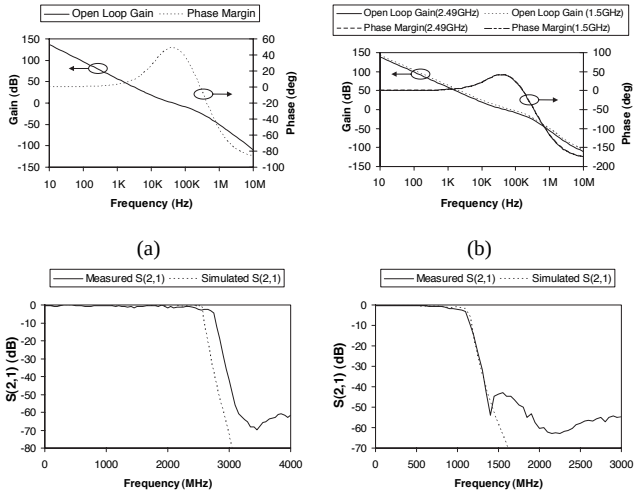

(a) (b)

(c) (d)

Figure 2: (a) 3rd Order Passive Loop Filter Design with ADS (b) 3rd Order Active Loop Filter Design with ADS. Measured and Simulated Filter Characteristics for (c) before mixer, (d) after mixer.

tor (TCXO), which is highly stable and produces an exact frequency. The locked frequency is controllable digitally by setting the dividing ratio. The oscillators generate not only fundamental signals but second, third, and higher order harmonics within the desired band. The LPF (low pass filter) after wideband oscillator subdues the harmonic signals within the desired band. Fig. 1(b) shows the topology of the signal generator.

2.1.1 Design of Phase Locked Loop

The VCO of the local oscillator has a 2.4–2.55GHz range by 0∼5V tuning voltage. This is compared with a 10MHz reference TCXO. The frequency synthesizer, LMX2347 from National Semiconductor, has a sufficient tuning voltage range for this VCO. If the charge pump of the frequency synthesizer has enough voltage range, then a passive filter should be used for the lower noise. The loop filter of the local oscillator is designed as 3rd order and 40KHz loop bandwidth (Fig. 2(a)). Simulation shows 40.75KHz of loop bandwidth and 49° of phase margin. Fig. 1(c) shows locked signal at 2.5GHz. The wideband VCO also should be locked to generate precise mixed frequencies. Since it has 1.5–2.49GHz range, the control voltage of LMX2347 must be extended up to 18V, and an active filter is required. The 3rd order active filter is used for loop filter. Fig. 2(b) shows designed loop filter within the band. The loop bandwidth and phase margin are 32.66KHz and 45.47° at 2.49GHz, and 49.66KHz and 45.42° at 1.5GHz.

2.1.2 Filter Design

Two filters are used, one before and one after the mixer. The pre-mixer LPF, which inputs from the wideband oscillator, should be designed for the 2.5GHz passband, whereas the post-mixer filter should filter out frequencies over 1GHz. For high frequency applications, microstrip line filters are widely used due to the availability of accurate analysis. The full wave analysis gives the best predicted filter frequency response results, although it takes long computing time. We designed the pre-mixer filter with ADS using equip-circuit models, which are less accurate but effective. Fig. 2(c) shows simulated and measured filter characteristics. For the post-mixer filter, microstip line filter would be too big due to the long wavelength of the lower frequency. On the other hand, lumped components (i.e., inductors and capacitors) are suitable for lower frequencies, but the 1GHz frequency range is still high, and they do not match our calculation of frequency response due to too many parasitic values at high frequencies. Our basic design is 11th Chebyshev with 0.1dB ripple at the passband, and we replaced and optimized ideal lumped components with measured 2-port S-parameters of high Q inductors and capacitors. Fig. 2(d) shows simulated and measured filter characteristics. The trend of filter characteristics is matched well, though simulation shows more loss at higher band.

2.1.3 RF Power

The photo detector has −45dBm sensitivity, and 20dBm power yields a 65dB detection range. The maximum available power of Mini-FDPM is around 21dBm. Fig. 3(a) shows the maximum available power within the frequency band.

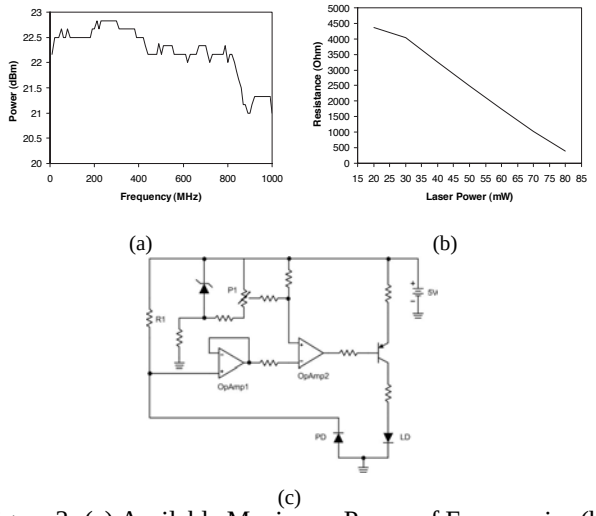

Figure 3: (a) Available Maximum Power of Frequencies (b) Measured Laser Power by resistance of digital potentiometer. (c) Topology of APC (automatic power control) circuit

2.2 Laser Driver

Given the same driving current, as the temperature increases, the laser power decreases. This means an ACC (automatic current control) circuit cannot maintain the precise laser power. Instead, we use an APC (automatic power control) circuit, which uses precise power monitoring feedback from photodiode right next to the laser diode, as shown in Fig. 3(c). It compares the voltage across R1 induced by the monitoring current from the photo diode with the voltage generated at the plus node of OpAmp2 by P1, a digital potentiometer. P1 continues changing value to control the driving current to the laser diode until the two voltages match. A to C of P1 is 5KΩ. Fig. 3(b) shows measured laser power by the resistance value of A to B.

3 Measurement Results

The measurement setup is shown on the right. The 783nm laser diode runs at 50mW. The Hamamatsu C5658 photo detector and the laser diode are attached 15mm apart on the phantom tissue. The laser is modulated 10MHz–1GHz in 10MHz steps with 15dBm power. Ten sampled points are taken and averaged at each frequency.

3.1 Device Compensation

The AD8302 (Analog Devices) outputs two voltage signals indicating the amplitude and phase differences between two input RF signals. Fig. 4(a) shows the voltage value

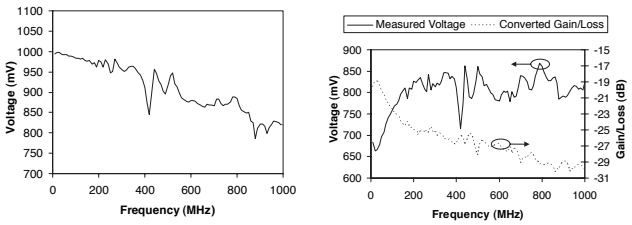

Figure 4: (a) Measured Gain/Loss Voltages with −30dBm reference signal (b) Converted Gain/Loss

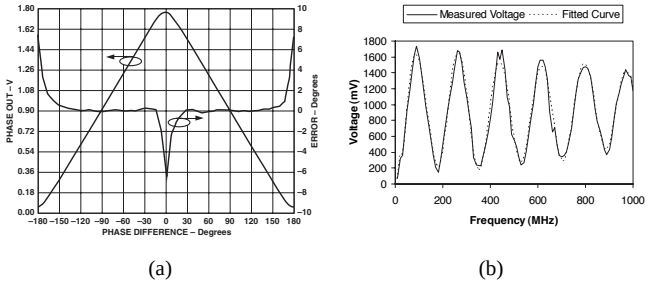

Figure 5: (a) Phase vs. Phase Voltage (b) Fitted Curve of 20th polynomial equation

of gain/loss with −30dBm input from the signal generator (Agilent 83650B). These measured voltages can be used as reference voltages and to derive the −1dB/+30mV slope of the detector. Fig. 4(b) shows the converted gain/loss results from measurement of an ISS2 tissue phantom. The rate of voltage vs. phase is 10mV/degree from measurement, but directly converting from rate can cause errors at maximum and minimum points, as shown in the Fig. 5(a). To avoid these errors, we detect the maximum and minimum points from the measurement voltages and convert to phase by setting minimum to 0° and maximum to 180°, but it is difficult to distinguish maximum and minimum points from measurement voltages directly due to noises. So, we made it a smooth curve with nonlinear least-squares fit using MATLAB. Once the fitted curve is found, the maximum and minimum points are easily calculated. Fig. 5(b) shows the measurement voltages from the ISS2 phantom and fitted curve by 20th polynomial equation.

3.2 Tissue Phantom Compensation

To compensate for device errors, we use the ISS2 tissue phantom, whose absorption and reduced scattering coefficients (μ_a and μ_s', in units of mm^{-1}) at λ =783nm are known to be 0.01405 and 0.35998, as derived based on diffusion theory and measurement data. The difference between derived and measured data is the calibration factor for new measurement. By removing the calibration factor, only the

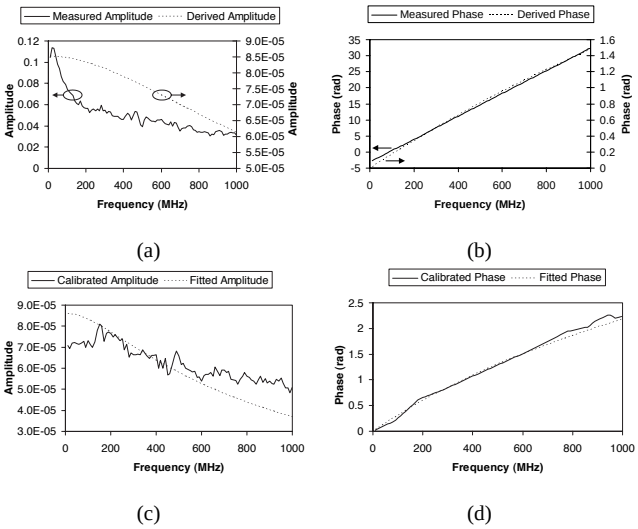

Figure 6: (a) Measured Amplitude vs. Derived Amplitude (b) Measured Phase vs. Derived Phase (c) Calibrated Amplitude Data vs. Fitted Data (d) Calibrated Phase Data vs. Fitted Data

phantom response can be recovered. Modified MATLAB code using diffusion theory in semi-infinite media with extrapolated boundary condition [7] from BLI is used to derive amplitude and phase response of ISS2 from optical properties. Fig. 6(a) and Fig. 6(b) show measured vs. derived amplitude and phase. The differences are calibration factors due to the device and measurement environment. To determine the calibration factors, one way is to subtract derived data from measured or to divide measured data by derived, and choose the best factors after several iterations. The best are cubed measured amplitude divided by derived amplitude and measured phase subtracted by derived phase.

3.3 Extracted Optical Properties

PH010, another phantom with known μ_a=0.00753 and μ_s'=0.903 at 783nm, is measured for the purpose of validating the accuracy of Mini-FDPM. We extract the measured optical properties of PH010 using the same MATLAB code from BLI. The measured data should be calibrated with calibration factors. Several iterations start with speculative initial absorption, and reduced scattering coefficients (μ_a and μ_s') were made to find minimum errors. Fig. 6(c) and Fig. 6(d) show the calibrated measurement data and best fitted amplitude and phase curve from theory. The extracted values from the fitted amplitude and phase curve are μ_a=0.00359 and μ_s'=0.759 for Mini-FDPM, vs. μ_a=0.0036 and μ_s'=0.954 for the LBS. In terms of percentage error, Mini-FDPM is μ_a=52.3% and μ_s'=13.9%, both are reasonably similar to the LBS, as shown in Fig. 7.

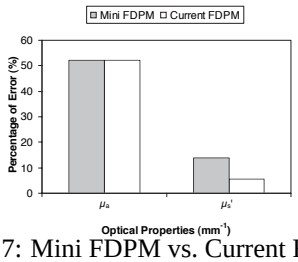

Figure 7: Mini FDPM vs. Current FDPM

4 Conclusions

This paper presents a miniature instrument for non-invasive, optical, content-based cancer detector based on FDPM. Our Mini-FDPM system performs active sensing by emitting a broadband modulated laser light and measures the backscattered light in terms of amplitude and modulation phase shift. To achieve the 10MHz–1GHz band by downmixing, we overcame challenges in broadband modulation by pre-mixer and post-mixer filter designs, as well as APC circuitry with a feedback signal to compensate for the temperature sensitivity. We have calibrated the instrument and demonstrated measurement results with a clinical phantom. The dramatically lower cost, form factor, and performance are expected to enable this non-invasive, effective breast cancer detection method to gain much wider use.

References

[1] B. J. Tromberg, N. Shah, R. Lanning, A. Cerussi, J. Espinoza, T. Pham, L. Svaasand, and J. Butler, "Non-invasive *In Vivo* characterization of breast tumors using photon migration spectroscopy," *Neoplasia*, vol. 2, no. 1–2, pp. 26–40, Jan.–Apr. 2000.

[2] E. C. Fear, P. M. Meaney, and M. A. Stuchly, "Microwave for breast cancer detection?" *IEEE Potentials*, 2003.

[3] X. Li and S. C. Hagness, "A confocal microwave imaging algorithm for breast cancer detection," *IEEE Microwave and Wireless Components Letters*, vol. 11, no. 3, March 2001.

[4] P. Meaney, M. Fanning, D. Li, S. Poplack, and K. Paulsen, "A clinical prototype for active microwave imaging of the breast," *IEEE Transactions on Microwave Theory and Techniques*, vol. 48, pp. 1841–1853, 2000.

[5] , "Using "radar" to detect breast cancer," *Microwave News*, March/April 2000.

[6] T. H. Pham, O. Coquoz, J. B. Fishkin, E. Anderson, and B. Tromberg, "Broad bandwidth frequency domain instrument for quantitative tissue optical spectroscopy," *Review of Scientific Instruments*, vol. 71, no. 6, pp. 2500–2513, June 2000.

[7] R. C. Haskell, L. O. Svaasand, T.-T. Tsay, T.-C. Feng, M. S. McAdams, and B. J. Tromberg, "Boundary conditions for the diffusion equation in radiative transfer," *Optical Society of America*, vol. 11, no. 10, pp. 2727–2741, October 1994.